scientific reports

Check for updates

OPEN

Biochar carbon nanodots for catalytic acetalization of biodiesel by-product crude glycerol to solketal: process optimization by RSM and life cycle cost analysis

Supongsenla Ao[1], Shiva Prasad Gouda[1], Lakshi Saikia[2], Baskar Gurunathan[3] & Samuel Lalthazuala Rokhum[1]✉

Carbon-based nanodots have garnered recent interest for their simple synthesis and versatile utility, ranging from biomedical to (opto) electronic applications, evolving into a tunable and biocompatible material. Here, for the first time, a biochar (lotus leaf) derived carbon nanodots was synthesized through hydrothermal carbonization. The synthesized hollow spherical biochar was engineered via functionalization by grafting –SO_3H active sites. The attained catalyst was broadly analyzed by XRD, FTIR, TGA, BET, SEM–EDX, TEM, and XPS analysis after which it was applied for the acetalization reaction of crude glycerol (a biodiesel by-product) to form solketal, a potential fuel additive to valorize the large waste stream generated from biodiesel industry. Employing the RSM-CCD methodology, the experimental matrix was executed, and subsequent data were scrutinized through multiple regressions to model a quadratic equation. Under specific reaction parameters—a reaction duration of 14 min, a molar ratio of 7.5:1, and a catalyst loading of 5.7 wt.%, maximum solketal yield (95.7%) was attained through the ultrasonication method. Finally, to conclude, life cycle cost analysis (LCCA) for solketal production was studied here which determined the overall cost of solketal production per kilogram to be 0.719 USD ($), indicating high commercial applicability.

Keywords Biochar, Carbon-nanodots, Acetalization, Solketal, Life cycle cost analysis

Carbon is widely abundant in nature and exists in various allotropic forms. Lately, there has been considerable attention towards carbon-based nanomaterials like carbon nanotubes (CNTs), graphene quantum dots (GQDs), and carbon nanodots (CNDs) owing to their straightforward manufacturing techniques and extensive range of possible uses. These applications span from the energy sector to biomedicine to (opto) electronics, with emerging uses as a tunable and biocompatible substance [1]. Consequently, the focus in green chemistry research has shifted towards converting carbon-based biowastes into sought-after carbonaceous nanomaterials. This involves harnessing the unique size, surface characteristics, and optical properties of these materials, leading to a diverse range of practical applications. Carbon nanodots (CDs), were first reported by Xu et al. [2] in 2004 during the purification of single-walled carbon nanotube (SWCNT), here spherical nanoparticles (< 10 nm) composed of sp^2 or sp^3 hybridized carbon atoms were observed [3]. They are generally non-toxic and biocompatible, which makes it easier for other functional groups to connect to them, like amines, carbonyls, epoxy, carboxylic, ethers, and hydroxyls. These groups can then be adjusted using standard synthetic techniques to alter their properties and use [4,5].

The recent trends in biofuel production due to the rapid depletion of fossil fuels have led to a tremendous increase in biofuel production. Fatty acid methyl ester also known as biodiesel, which is attained by

[1]Department of Chemistry, National Institute of Technology Silchar, Silchar 788010, Assam, India. [2]Advanced Materials Group, Materials Sciences and Technology Division, CSIR-North East Institute of Science and Technology, Jorhat 785006, Assam, India. [3]Department of Biotechnology, St. Joseph's College of Engineering, Chennai 600119, India. ✉email: rokhum@che.nits.ac.in

transesterification of vegetable oil/ animal fats in the vicinity of a catalyst is a renewable and alternative fuel to petroleum fuel (Fig. 1) [6,7]. It is considered one of the best substitutes for petroleum fuel due to its unique chemical structure. Each fatty acid methyl ester (FAME) molecule contains an ester group (–COO–) that has oxygen within it which helps in complete combustion of the fuel resulting in reduced emissions of hydrocarbons and carbon monoxides [8,9]. However, to keep in mind, it has been reported that for every 100 kg of biodiesel produced, 10% of glycerol has been generated as a by-product [10,11]. This increasing production of glycerol, following refinement, exceeds its industrial value, leading to a significant decline in its market price. Consequently, this raises doubts about the sustainability of the biodiesel industry. Therefore, it is crucial to focus on innovative approaches to enhance the utilization of glycerol.

A series of tractable processes such as transesterification [12], esterification [13], polymerization [14], etherification [15], acetalization [16], carbonylation [17], and oxidation [18] are some of the methods opted for valorizing the byproduct glycerol. Solketal, a five-membered heterocycle known as 2,2-dimethyl-1,3-dioxolane-4-methanol compound obtained by the acetalization process of glycerol (Fig. 2) holds significant commercial value and is widely utilized as a fuel additive. It has the potential to enhance the octane rating and cold flow characteristics of transportation fuels, while also reducing particulate emissions and gum formation during fuel combustion. In addition to these advantages, solketal finds applications in various other industries, acting as a plasticizer, suspending agent, surfactant, and flavoring agent, in the pharmaceutical sector.

Recently reported silica-coated Fe_3O_4 magnetic nanoparticle catalyst by Rajkumari et al. [19] for the production of solketal (95% yield) was reused up to five reaction cycles which was possible due to the magnetic properties. In

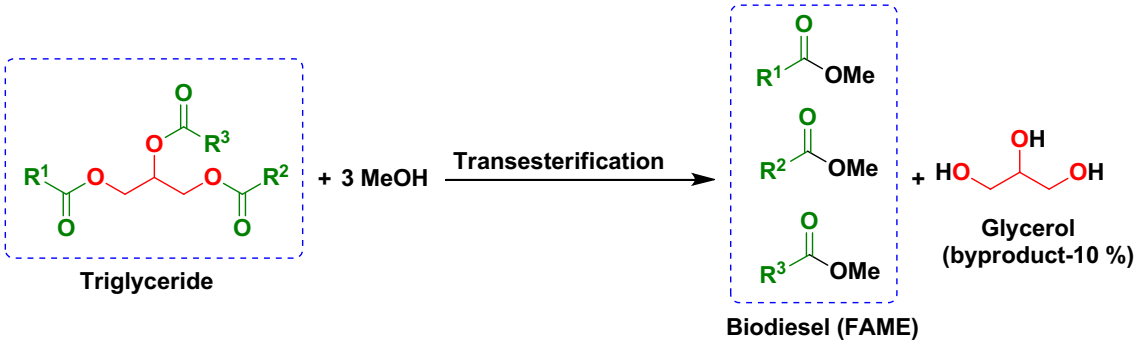

Figure 1. Transesterification reaction of triglyceride to form biodiesel.

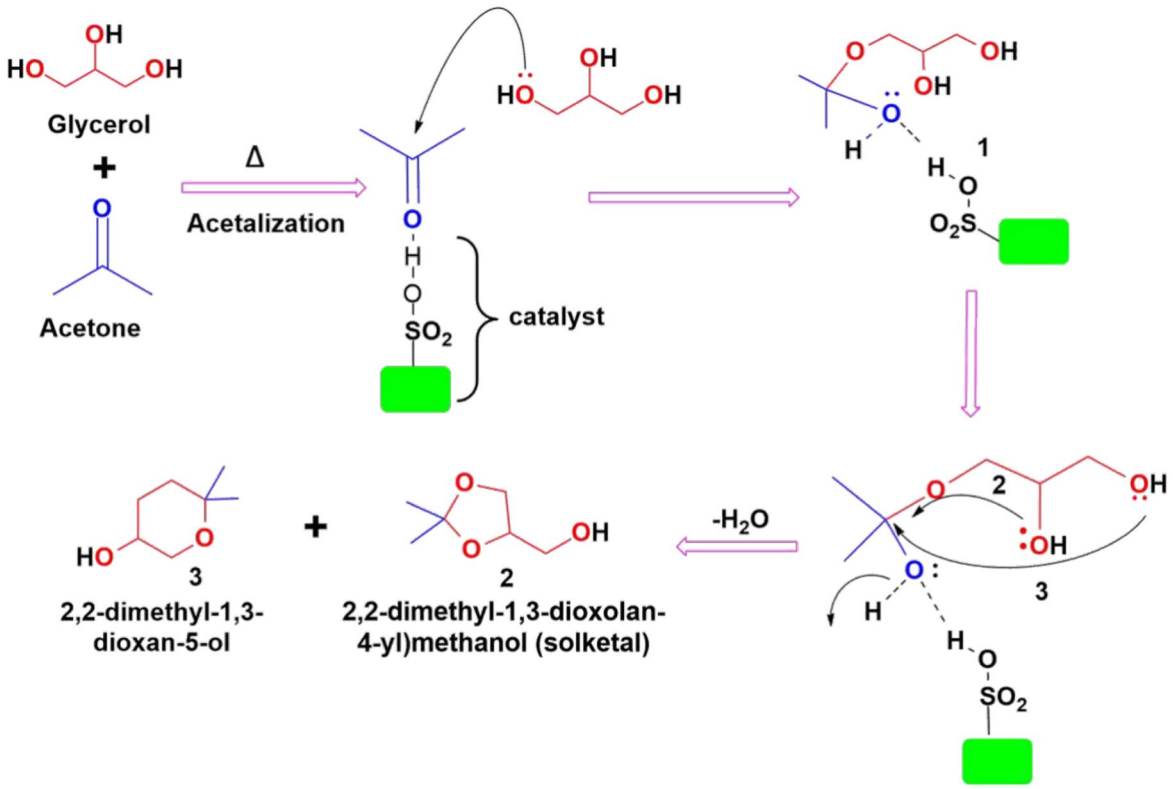

Figure 2. Acetalization reaction mechanism of biodiesel by-product glycerol.

another work by Laskar et al. [20] a PSF-resin (polysulfonic acid resin) catalyst gave a high glycerol conversion of 97% with 100% selectivity to solketal which was ascribed to high Bronsted acid sites and porous structure of the polymeric catalyst. In 2021, Huang et al. [21] synthesized WO_X/MCM-41 catalyst by wet impregnation method. The catalyst was later utilized in the ketalization of glycerol to solketal giving 73.84% yield using 10 wt.% catalyst. To lay the foundation for the advancement of glycerol valorization techniques, focus on commercial catalysts such as Amberlyst-35 [22], Amberlyst 15 [23], and zirconium oxide sulfated [24], were also explored towards the conversion of glycerol into solketal, with special consideration for sorption-enhanced reactive methodologies, which are recognized as among the most favorable approaches for such systems.

Our recent investigations on the valorization of crude glycerol (a by-product of biodiesel) to solketal have been investigated by synthesizing highly efficient and novel catalysts from resins [20] (PSF-resin) to magnetic catalyst [19] (silica-coated Fe_3O_4 magnetic nanoparticle) and lately shifting to biomass-derived catalysts such as C–SO_3H [16], and SAFACAMs [10] have proved to be quite successful in synthesizing the fuel additive solketal. Despite such advancements, our synthesized catalysts remain unstable after 4–5 reaction cycles. The main reason for the decline in activity was attributed to the formation of carboxylate and sulphonate esters, which occur when the carboxylic acid and sulfonic acid sites react with glycerol [10,16].

With all these considerations in mind, our present research aims to create spherical biochar composed of carbon nanodots, derived from lotus leaf extract using a straightforward hydrothermal treatment (Fig. 3). This resulting biochar underwent functionalization by H_2SO_4 to introduce active sites (–SO_3H) uniformly across the catalyst. Due to their consistent spherical shape and superior ability to facilitate mass transfer, spherical biochar catalysts exhibit enhanced performance in chemical processes, leading to improved catalytic efficiencies. Significantly, this is the first reported instance of utilizing such a biochar-derived carbon nanodot catalyst for the acetalization of crude glycerol to produce solketal, a promising fuel additive. Further, a response surface methodology-central composite design (RSM-CCD) was then adopted to optimize the complex interplay of process factors such as time, molar ratio, and catalyst activity, aiming to enhance solketal yield efficiently. Finally, our study investigated the life cycle cost analysis (LCCA) of solketal production to determine its efficiency and

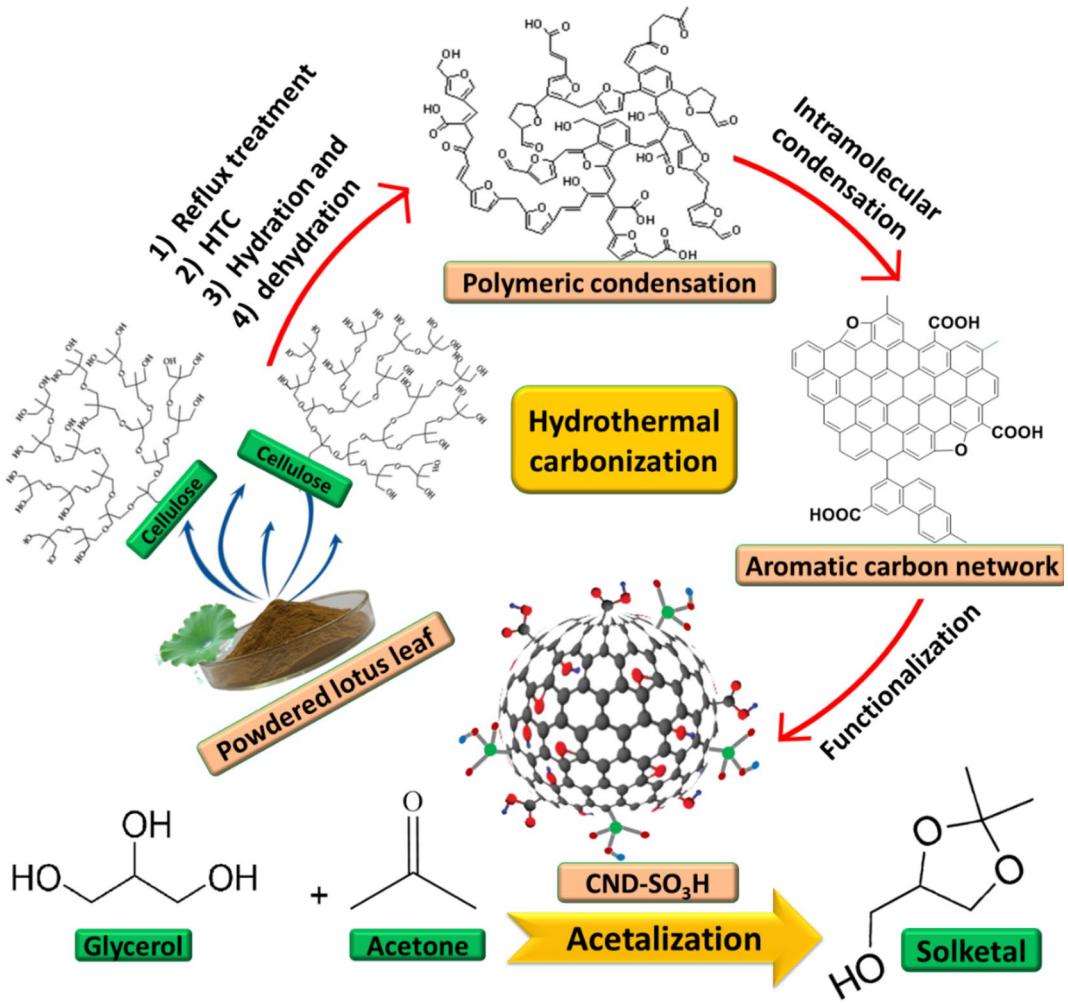

Figure 3. Schematic representation of hydrothermal carbonation of our biochar catalyst for acetalization reaction.

affordability, recognizing its significant influence on the feasibility and cost-effectiveness of large-scale production. The synthesis and extraction of environmentally friendly carbon nanodots (CNDs) from natural sources, particularly food and plant waste, represent a heavily studied area aligned with the principles of the circular economy. The combination of the process of waste management with the synthesis of CND particles promotes environment-friendly and scientifically innovative sustainable solutions.

Experimental

Materials used

Acetone (98.5%), pH paper, silica powder (325 mesh), methanol (99%) H_2SO_4 (98.07% purity), $BaCl_2$ (99.95%), were acquired from India Mart, Sisco Research laboratory. Chemicals were utilized without any prior purification. Lotus leaf (*Nelumbo nucifera)* was collected from the institute campus of NIT Silchar, Assam, India (24.75° N, 92.79° E). Further, crude glycerol (properties tabulated in Table S1) obtained from biodiesel production was purchased from Karma Biofuels, India Mart. We have acquired the necessary permissions to gather the biomass, ensuring that this study adheres to the appropriate institutional, national, and international guidelines and regulations.

Catalyst preparation

Carbon nanodots (CNDs) was synthesized through a hydrothermal treatment of lotus leaf extract as illustrated in Fig. 4. In this procedure, 10 g of powdered (sieved using 150 mesh size sieve) lotus leaves along with 200 mL of DI water were added one after the other in a Soxhlet apparatus, and the reaction mixture was heated to 80 °C for a duration of 12 h. The yellowish extract (180 mL of total 200 mL DI water used) was filtered and collected in a beaker. Subsequently, 150 mL of the filtered lotus leaf extract was transferred to a Teflon-lined stainless-steel autoclave and subjected to hydrothermal treatment at 180 °C for 24 h. After the reaction, the autoclave was allowed to cool naturally to room temperature. The obtained CNDs was washed down with distilled water (2×15 mL) and collected through centrifugation at 4000 rpm for 10 min.

For functionalization, 0.5 g of CNDs was dissolved in 5 mL of H_2SO_4 (1:10 wt./mL). The mixture was then heated in a hot air oven at 100 °C for 24 h, after which it was cooled to room temperature, and rinsed with

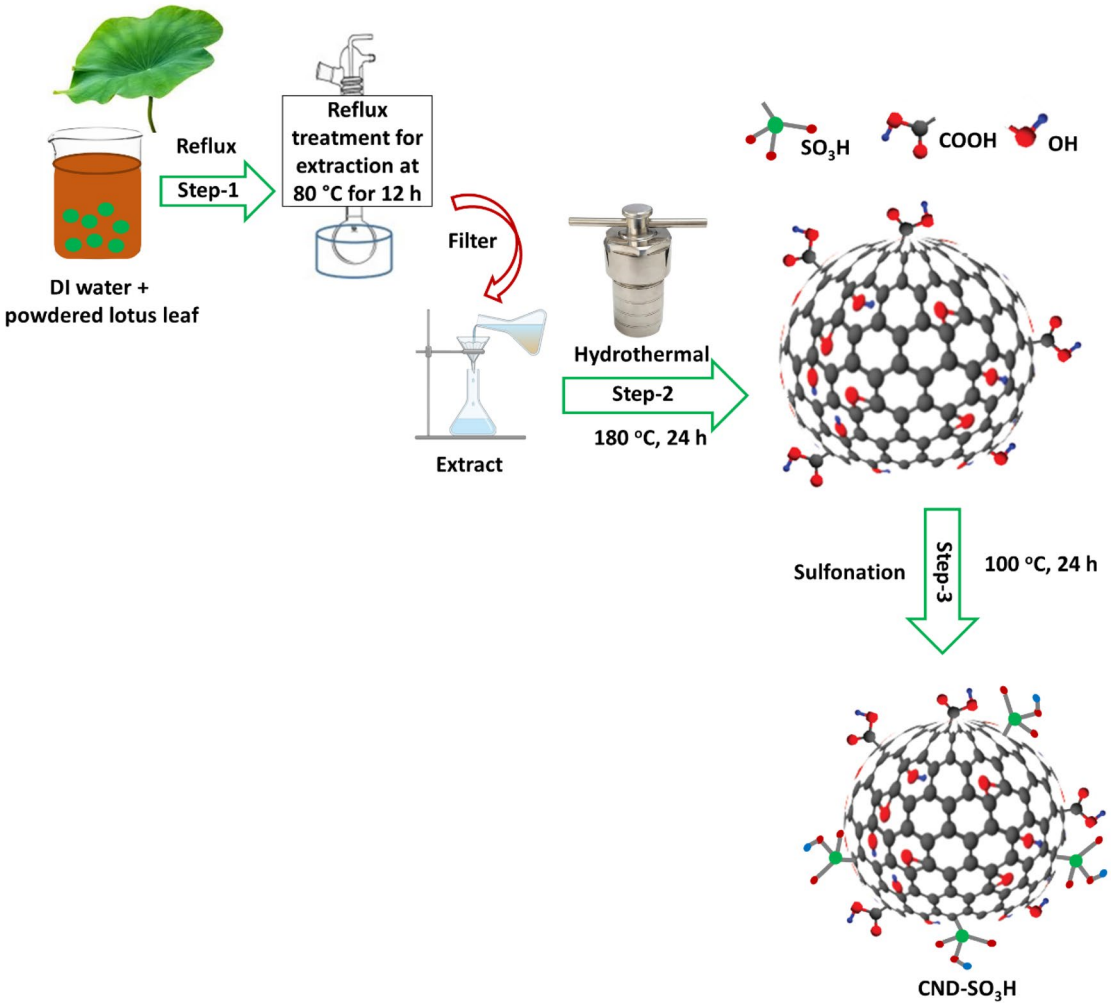

Figure 4. Pictorial representation of step wise preparation for CND-SO_3H catalyst.

deionized water until sulfate ions were undetectable by giving a clear solution (verified by $BaCl_2$ test- under 6 mol/L $BaCl_2$ solution [25]). The resulting product, sulfonic acid-functionalized carbon nanodots (CND-SO_3H), was kept for drying overnight at 80 °C in an oven and stored for use.

Characterization of the catalyst

The total acid density on CND-SO_3H was evaluated employing the Boehm titration method [26]. The comprehensive acid density was determined using NaOH solution. Equation (1) was employed to compute the total surface acid density of the catalyst.

$$n = \frac{n_{HCl}}{n_B}[B]V_B - ([HCl]V_{HCl} - [NaOH]V_{NaOH})\frac{V_B}{V_{aliquot}} \quad (1)$$

where, $\frac{n_{HCl}}{n_B}$ is the molar ratio of HCl to base reacted; $[B]$, the concentration and volume of the reaction base mixed with the catalyst are denoted as V_B and V_C respectively. $V_{aliquot}$ represents the volume of the aliquot taken from V_B. Furthermore, [HCl] and V_{HCl} stand for the concentration and volume of acid used in the acidification process, while [NaOH] and V_{NaOH} represent the concentration and volume of NaOH used in the titration.

X-ray diffraction (XRD) analysis utilized a PANalytical X'Pert Pro diffractometer, employing Cu Kα radiation in the 2θ range of 20–100°, with operational parameters set to 40 kV and 100 mA for voltage and current, respectively. Next, Fourier-Transform Infrared (FTIR) spectra were acquired using a 3000 Hyperion FTIR spectrometer (Bruker, Germany) spanning the range of 400–4000/cm to discern functional groups within the elements. Following, thermogravimetric analysis (TGA) of the catalyst was done using a TG/DTA instrument (model no. STA 409 Netzsch Geratebau GMBH, Germany) under airflow at 1.5 bar and 2 L/h, with degassing temperatures ranging from 50 to 800 °C. Evaluation of the catalyst's size, shape, and elemental composition involved scanning electron microscopy (SEM) and energy-dispersive X-ray spectroscopy (EDS). SEM analysis was conducted using a JEOL JSM-7600F instrument, with SEM images captured using the FEI Quanta 200 F instrument equipped with a tungsten-doped lanthanum hexaboride (LaB6) X-ray source and an ETD detector under high vacuum conditions and utilizing secondary electrons at a 30 kV acceleration voltage. Transmission Electron Microscopy (TEM) images and selected area electron diffraction (SAED) patterns were obtained using an HR-TEM JEOL instrument (JEM 2100, 200 kV), samples were prepared by dropping an aqueous solution of carbon dots on a carbon-coated copper grid. Before the Brunauer–Emmett–Teller (BET) method application, the catalyst underwent a 10 h degassing at 150 °C on a Micromeritics ASAP 2010 surface area and porosity detector, and N_2 adsorption–desorption isotherms were calculated using the same analyzer. X-ray photoelectron spectroscopy (XPS) analysis utilized an ESCALAB Xi + system with a micro-focused dual-anode Al/Mg K source, with samples heated to a maximum temperature of 50 °C at a rate of 5 °C/min and a helium flow of 100 cm^3/min.

Acetalization of glycerol to form solketal

A reaction mixture of glycerol (2.5 mmol), acetone (12.5 mmol), and a catalyst loading of 8 wt. % (0.018 g) was set in a 50 mL round bottom flask for ultrasonication under a 700-W bath for 20 min. After the reaction was complete (verified by TLC), the catalyst was filtered out. Excess acetone from the filtrate was evaporated using a rotary evaporator to obtain the product. Mean glycerol conversions were determined from three distinct catalytic experiments. The resultant product underwent comparison with previously reported solketal syntheses [16,19,20] and was examined through gas chromatography and/or NMR spectroscopy. Gas chromatography (GC) analysis utilized a GC-flame ionization detector (GC-FID) to identify the product. The oven temperature was set from 55 to 230 °C at a rate of 10 °C/s. In addition, deuterated solvent $CDCl_3$ was used to run ^1H and ^{13}C NMR spectroscopy of the reaction product on a Bruker Avance II 500 MHz spectrometer at 28 °C. Equations (2) and (3) were used in GC–MS to verify the conversion of glycerol and the selectivity of solketal production (vs. 2,2-dimethyl-1,3-dioxan-5-ol).

$$\text{Glycerol conversion (\%)} = \frac{Mol\ glycerol\ converted}{Initial\ mol\ glycerol} \times 100 \quad (2)$$

$$\text{Solketal selectivity (\%)} = \frac{Mol\ solketal\ formed}{Mol\ glycerol\ converted} \times 100 \quad (3)$$

Response surface methodology

RSM stands out as a reliable approach to investigating the impact of various parameters on a chemical reaction. Stat-Ease Inc.'s Design Expert version 13.0 software from Minneapolis, Minnesota, USA, was applied for the model's regression analysis. The high and low values were selected based on the experimental observations (trial and error) of each parameter and provided in the Design expert software. The experiment examined various factors—ace:gly (molar ratio) ranged from 4:1 to 8:1, catalyst loading ranged from 4 to 6 wt.%, and reaction time ranged from 11 to 15 min. To ensure result consistency, a factorial design with five levels and four factors was used, along with six center points, minimizing variability's impact. The analysis employed multiple regression to define a quadratic model for the response based on the experimental data. To uncover the intricate relationships and dependencies among these variables, we meticulously designed a total of 20 experiments (Table 1), following the equation $2^n + 2n + 6 = 20$.

Std	Run	Space type	A: Ace:Gly (Molar ratio)	B:Time (min)	C: Cl (wt. %)	Actual value	Predicted value
19	1	Center	6	13	6	92.1	87.87
4	2	Factorial	8	15	4	86.1	89.03
8	3	Factorial	8	15	8	92.4	92.71
9	4	Axial	3	13	6	62.2	63.8
11	5	Axial	6	10	6	78.1	77.23
20	6	Center	6	13	6	84.3	87.87
6	7	Factorial	8	11	8	80.3	83.69
1	8	Factorial	4	11	4	58.4	59.24
5	9	Factorial	4	11	8	70.2	68.43
7	10	Factorial	4	15	8	65.3	66.84
3	11	Factorial	4	15	4	76.2	73.96
18	12	Center	6	13	6	90.1	87.87
17	13	Center	6	13	6	84.5	87.87
13	14	Axial	6	13	3	68.1	67.85
15	15	Center	6	13	6	86.3	87.87
14	16	Axial	6	13	9	79.3	77.5
10	17	Axial	9	13	6	90.2	86.55
12	18	Axial	6	16	6	96.2	95.02
2	19	Factorial	8	11	4	64.1	63.71
16	20	Center	6	13	6	88.4	87.87

Table 1. Design matrix, featuring experimental factors (A–C) and their associated actual and predicted yields for the acetalization reaction.

Utilizing the quadratic polynomial equation (Eq. 4), we sought to evaluate how these components performance and their interactions impact production efficiency, with the ultimate goal of identifying the optimal response.

$$Y = \alpha_0 + \alpha_1 A + \alpha_2 B + \alpha_3 C + \alpha_{12} AB + \alpha_{13} AC - \alpha_{23} BC - \alpha_{11} A^2 \alpha_{22} B^2 - \alpha_{33} C^2 \quad (4)$$

In this particular context, Y stands for the solketal yield derived from glycerol, which is the primary response of concern. The intercept term is symbolized as α_0, whereas α_1 to α_3 represent the coefficients associated with the linear terms. For the interaction terms, we use α_{12}, α_{13}, and α_{23}, while α_{11}, α_{22}, and α_{33} correspond to the coefficients for the quadratic terms. Factors A, B, and C are coded as such in this analysis.

Test for heterogeneity test and reusability

Heterogeneity test was conducted through the Hot Sheldon filtration technique [19] to verify the heterogeneity of the catalyst. Following a 10-min interval, the catalyst and reaction mixture were separated allowing the reaction to proceed independently for another 10 min without the catalyst. TLC was used to monitor the progression of the reaction.

After each reaction cycle, the catalyst underwent a separation process from the reaction mixture through filtration. Subsequently, it was alternately rinsed three times with 15 mL of acetone. After this rinsing procedure, the recovered catalyst was subjected to a 5 h drying period in a hot air oven set at 80 °C. The weight of the catalyst in its dry state was measured before its subsequent use, and it is important to mention that there was no significant change in mass observed during any of these steps.

Results and discussions

Total acidity test using Boehm titration

A quantity of 100 mg of the catalyst was mixed into 40 mL of 0.05 M NaOH solution and agitated for 24 h. Following this, the solution was filtered, and a 10 mL sample was removed and neutralized with 20 mL of a 0.05 M HCl solution at a standard concentration. Phenolphthalein indicator was then added, and the mixture was subsequently titrated using a standardized 0.05 M NaOH solution. Using Eq. (1), the total acidity of the catalyst was calculated to be 1.38 mmol/g.

Characterization of synthesized catalyst

The prepared catalyst was studied using various analytical techniques to verify the nature of the catalyst. The XRD analysis of the catalyst (Fig. 5a) aligns with recent findings, suggesting that the biomass extract underwent carbonization, resulting in the formation of amorphous carbon [10]. Verification of functionalization, involving the introduction of hydrophilic –COOH (1670/cm) and –OH groups (3405/cm), along with $-SO_3H$ active sites onto the polycyclic aromatic carbon of CNDs, was confirmed through FT-IR analysis (Fig. 5b) [9]. The presence of $-SO_3H$ functional group after sulfonation of CND was further confirmed by the emergence of the characteristic

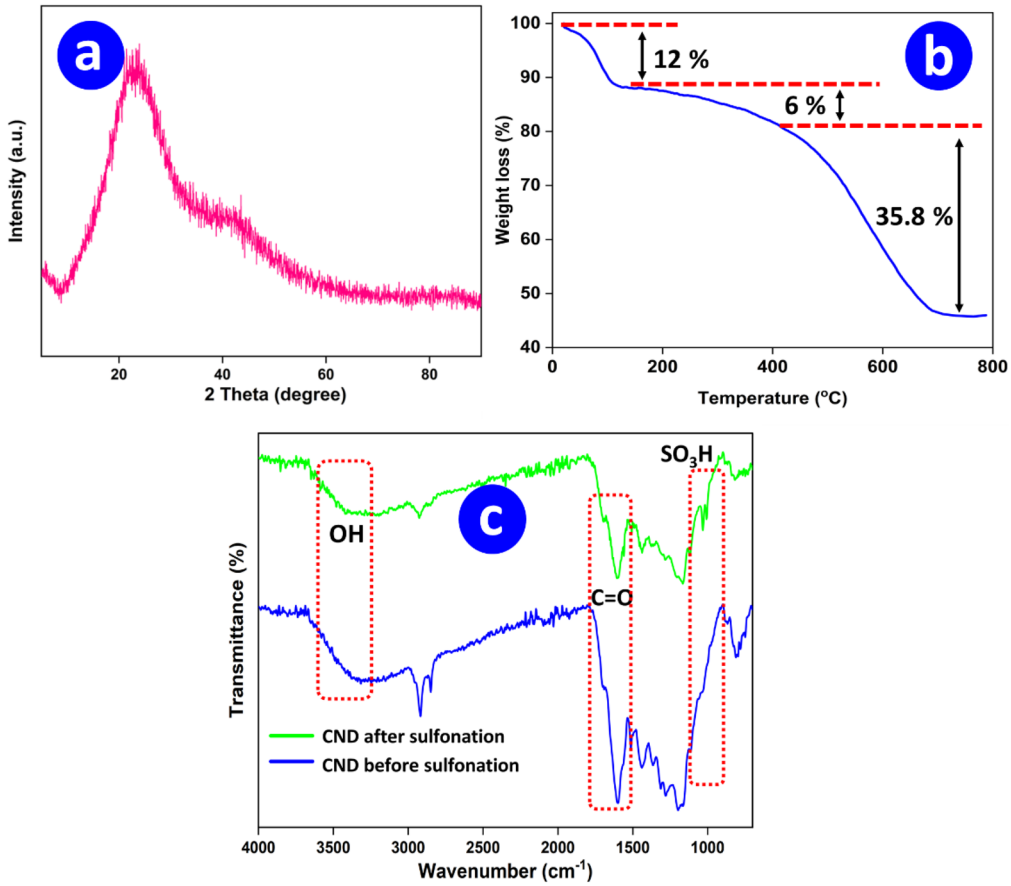

Figure 5. XRD pattern (**a**), (**b**) TGA lines, and (**c**) FT-IR spectrum (showing successful sulfonation) of the current, as-prepared CND-SO_3H catalyst.

stretching vibration of S=O and S–O at 1100/cm and 1020/cm [27] in the FTIR graph which was absent in the plot (blue graph) which was done before sulfonation. The thermogravimetric analysis (TGA) data (Fig. 5c) indicates an initial 12% reduction in mass between 50 and 70 °C, attributed to the removal of adsorbed water. Subsequently, the catalyst exhibited stability up to 250 °C beyond this point, and the 6% decomposition of functional groups was observed, as reported in reference [28]. A subsequent decline in mass above 400 °C primarily resulted from the oxidation of the catalyst's carbonaceous structure, leading to the release of compounds like CO and CO_2, as explained in reference [29]. After 680 °C, there was no further observed mass loss, and a residual mass of 46.12% (1.264 mg) was determined from the initial total mass of 2.7408 mg.

CND-SO_3H was studied under SEM analysis to display a spherical structure (Fig. 6a–f) comparable structure reported in previous literature [30]. EDS analysis in Fig. 6g, h shows the sample's compositional homogeneity. Here, Fig. 6g shows the elemental composition of carbon nanodots before sulfonation and Fig. 6h shows the elemental composition after sulfonation which records 1.81 wt.% sulfur. TEM micrographs (Fig. 7a–e) provide a closer examination of the CND-SO_3H, revealing their spherical shape. This characteristic is evident in the higher magnification images (Fig. 7a, b). The SAED pattern (Fig. 7c) illustrates diffused rings, indicating the amorphous nature of the material, with an interplanar distance (d) calculated to be 0.2 nm (Fig. 7e). Additionally, the average particle size of the CND-SO_3H was determined to be 18.6 nm, as depicted in the particle size distribution curve (Fig. 7f).

The BET characteristics of the present catalyst encompassed both micro and mesoporosity. Consequently, nitrogen adsorption–desorption analysis was carried out to investigate the surface area and average pore size of the CND-SO_3H catalyst. The findings, displayed in Fig. 8 exhibit a hysteresis loop typical of a type-IV isotherm and H2b hysteresis loop, indicating internal narrow pore entrances [31]. Through BET analysis, the surface area, pore volume, and mean pore diameter of the current catalyst were determined to be 24.9 m^2/g, 0.24 cc/g, and 3.6 nm, respectively. These results demonstrate a satisfactory comparison with prior research [32].

The XPS analysis confirmed the presence of carbon (C), oxygen (O), and sulfur (S) in the survey spectrum (Fig. 9a). Notably, the deconvoluted C1s spectrum (Fig. 9b) revealed prominent peaks at 283.6 and 287.0 eV, corresponding to C=C and COOH [9], respectively. Additionally, the O1s spectrum (Fig. 9c) displayed peaks for C–O and C=O at 531.3 and 529.4 eV, respectively. Examination of the S2p area (Fig. 9d) revealed significant peaks at 166.0 and 167.1 eV appeared due to the possibility of spin–orbit coupling in S2p, aligning with our prior research attributing these data to the presence of high oxidation state (+6) sulfur in –SO_3H [33].

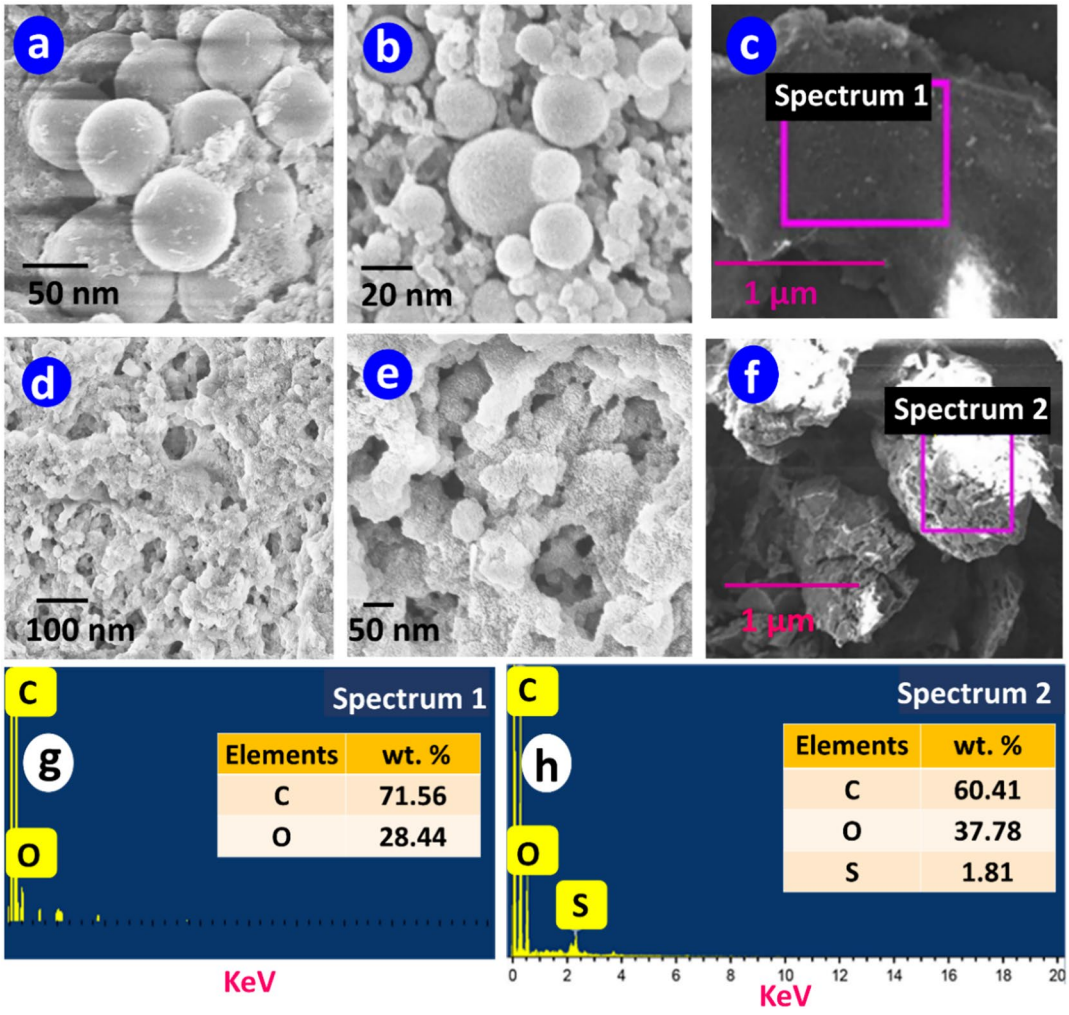

Figure 6. Representative SEM micrographs of CNDs (**a**–**c**) and CND-SO_3H catalyst (**d**–**f**). Scale bars 1 µm, 100 nm, 50 nm, 20 nm, and 5 nm. EDS data for the pink-boxed area (**g** and **h**) of images (**c** and **f**) attributed to CND before and after sulfonation (CND-SO_3H).

Analysis of CCD- technique

Exhibition and evaluation of data using RSM

RSM was applied to explore the relationship between response (% solketal yield) and reaction variables A to C, as detailed in the "Parametric optimization by response surface technique (RSM)" section. The CCD method, employing a partial factorial design with amplified center and axial point gathering, enables the assessment of non-linearity within the expected model. The number of experiments (N) for CCD advancement is calculated using the formula $N = 2^n + 2n + m$, where n represents the independent variables and m accounts for replicated central points. Presently, the system involves $n = 3$ and $m = 6$, resulting in 20 tests conducted. These tests constitute eight cube points, six axial points, and six repeated center data, which are then analyzed randomly. Throughout these experiments, the solketal yield ranged from 58.4 to 94.1%. The relationship between glycerol and solketal yield is depicted in Eq. (1).

$$\begin{aligned}\text{Solketal yield (\%)} &= 87.78 + 7.74\,A + 5.52\,B + 3.38\,C + 2.40\,AB \\ &\quad + 2.95\,AC - 4.33\,BC - 5.44\,A^2 - 1.04\,B^2 - 6.55\,C^2\end{aligned} \tag{5}$$

where, 'A' denoted acetone to glycerol molar ratio, 'B' as catalyst loading (wt. %), and 'C' as the reaction time.

The experimental data underwent thorough analysis, employing a quadratic equation fitted through multiple regressions to understand the relationship between various variables and solketal yield. The impact of these variables was rigorously examined using analysis of variance (ANOVA). Detailed results of this analysis, specifically for glycerol-derived solketal yield, can be found in Table 2. The assessment of the model significance and the individual parameter effects on the response was concluded by evaluating the F-value of the regression model. Remarkably, the calculated F-value was approximately 257.29, highlighting the robustness of the model. Moreover, the obtained p-value of < 0.0001 indicates an exceedingly low probability of error, reinforcing the robustness of the analysis. It's worth noting that values below 0.05 are considered statistically significant, underscoring the reliability of the results. As delineated in Table 2, the linear terms (ace:gly molar ratio, catalyst loading, and time)

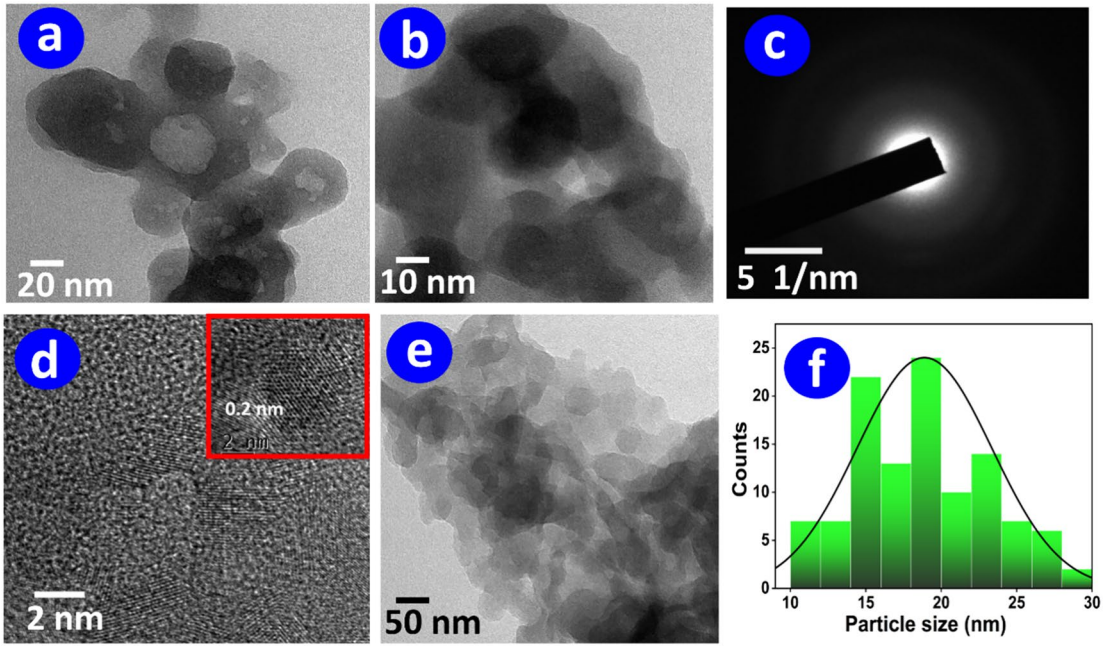

Figure 7. Representative TEM images of the catalyst (**a**, **b**, **d**, **e**) and SAED imaging (**c**) of the catalyst CND-SO_3H. Scale bars: 20 nm (**a**), 10 nm (**b**), 2 nm for panel (**d**), 50 nm for panel (**e**), and 5 1/nm (**c**). Additionally, an average particle size distribution graph of (**e**) is provided in panel (**f**).

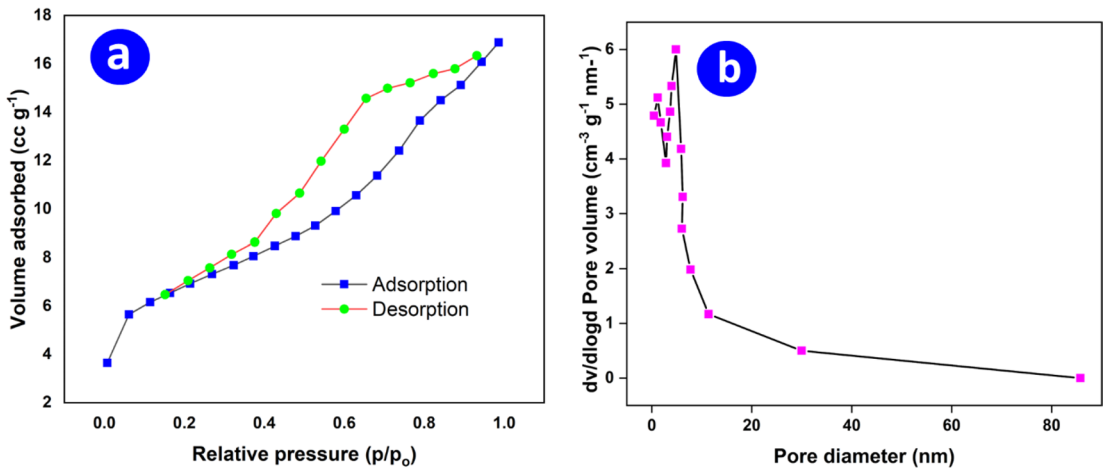

Figure 8. (**a**) N_2 adsorption–desorption isotherm and (**b**) BJH pore size distribution curve of CND-SO_3H catalyst.

and interactive terms were deemed significant. Additionally, the catalyst loading, reaction time, and quadratic terms (A^2, B^2, and C^2) exhibited negative coefficients in Eq. (4), suggesting a diminishing effect on the actual yield after reaching a peak at the midpoint values. In this context, A, B, C, AB, AC, and BC are significant model terms. Notably, values exceeding 0.1 in Table 2 denote that the model terms are not significant.

The predicted R^2, adjusted R^2, and adequate precision were three statistical measures that were used to estimate the accuracy of the regression equation. The predicted R^2 of 0.83 is in reasonable agreement with the adjusted R^2 of 0.93 indicating a difference of less than 0.2. The adjusted R^2 holds significance as it serves as a pivotal statistical gauge for evaluating the regression model's goodness of fit, surpassing the conventional coefficient of determination by accommodating the model's complexity. The coefficient of determination R^2 value of 0.9639 revealed the high correlation of the experimental data through the selected model. The model offers a good degree of accuracy with a sufficient precision value of 16.6 (ideally above 4) [34]. The obtained value suggests an adequate signal strength, affirming the usefulness of the regression model in guiding experimental outcomes within the designated parameters. Additionally, the coefficient of variation (CV) stands at a low 3.7%, highlighting a strong correlation between the observed and predicted outcomes, as values below 10% are indicative of a significant correlation [35].

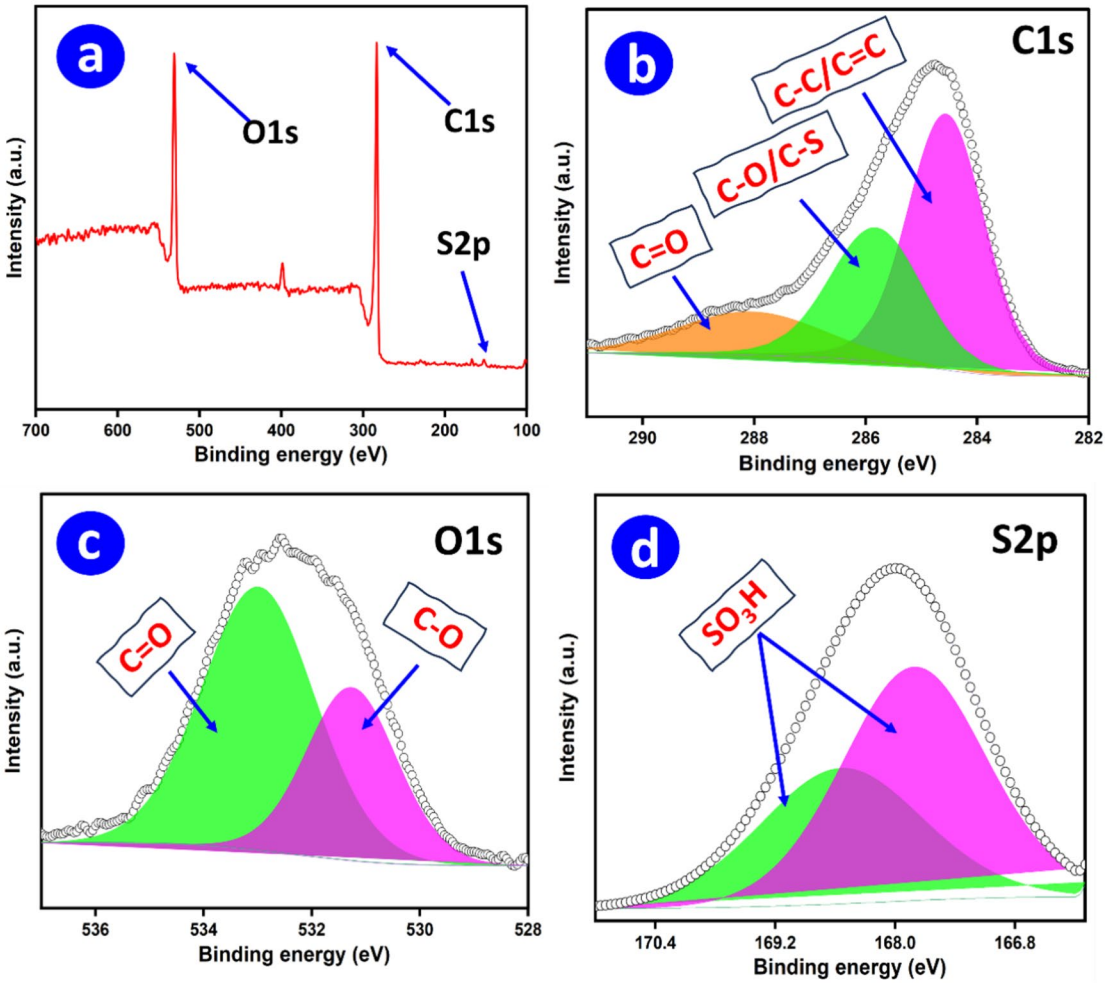

Figure 9. The XPS analysis survey spectrum result (**a**) along with the deconvoluted XPS signals (in orange, green, and pink) along with the raw data (shown in white bubbles) for the C1s (**b**), O1s (**c**), and S2p (**d**) region of the CND-SO_3H catalyst were analyzed.

Source of variance	Sum of squares	df	Mean square	F value	P value	Remark	Accuracy test	
							Parameters	Values
Model	2315.64	9	257.29	29.67	< 0.0001	Significant	R^2	0.96
A-Ace:Gly	749.62	1	749.62	86.46	< 0.0001		Adjusted R^2	0.93
B-Time	380.88	1	380.88	43.93	< 0.0001		Predicted R^2	0.83
C–Cl	142.47	1	142.47	16.43	0.0023		Adequate Precision	16.61
AB	46.64	1	46.08	5.31	0.0439			
AC	69.62	1	69.52	8.03	0.0177			
BC	149.64	1	148.64	17.26	0.0020			
A^2	305.13	1	305.13	35.19	0.0001			
B^2	11.18	1	11.18	1.29	0.2827			
C^2	442.47	1	442.47	51.03	< 0.0001			
Residual	86.70	10	8.67					
Lack of Fit	37.38	5	7.48	0.7577	0.6159	Not significant		
Pure Error	49.33	5	9.87					
Cor Total	2402.35	19						

Table 2. ANOVA and statistical results of regression model for the acetalization of glycerol.

The effectiveness of the regression model developed in this study was assessed through diagnostic plots, as depicted in Fig. S1(a–d). In Fig. S1a, the comparative analysis of the actual and predicted values reveals a high degree of alignment, indicating a minimal discrepancy. This close correlation between actual and predicted response values substantiates the robustness of the RSM-CCD approach and validates its predictive accuracy in determining the optimal yield of solketal. Figure S1b depicts a plot where studentized residuals are plotted in relation to the predicted yield. The observations demonstrate that the residuals scatter arbitrarily throughout the plot and stay confined within a threshold of ± 4.14. This pattern of distribution also suggests that the residuals do not display any systematic bias in relation to the predicted values. In Fig. S1c the residual vs. run plot for all the experimental runs shows that the residuals are scattered without displaying discernible patterns, which is indicative of their independent distribution. Ideally, in such plots, residuals are expected to be randomly distributed around the central line to suggest model precision [36]. The points in Fig. S1c confirm to this expectation, lying randomly around the central line and within established boundaries of ± 4.14.

The perturbation plot (Fig. S1d) illustrates how process factors impact solketal yield while keeping other variables constant [37]. Curvature characteristics in these plots reflect the fluctuation of A–C components on solketal yield, with steeper slopes indicating a stronger effect [38]. ANOVA Table S1 and Fig. S1d confirm that the acetone to glycerol ratio (A) shows the most abrupt slope change, followed by C and B. This is further supported by factor A having the highest sum of squares in the ANOVA study. Factor A significantly influences solketal yield from intermediate to higher levels, being most sensitive from lower to middle levels and slightly diminishing towards higher levels, while factors C and B exert notable effects from middle to higher levels.

The three-dimensional (3D) surface plots depict deeper insights into the individual and combined relationships influencing solketal yields. The interaction among these three variables is shown in Fig. 10. Notably, the variable ace:gly molar ratio emerged as a significant parameter. Examination of the surface graphs revealed that altering this ratio within the range of 4–8 molar ratio led to an increase in solketal yield, despite the concurrent increase in time, forming a hyperbolic plane (Fig. 10a). This occurrence is ascribed to acetone saturating active sites, thereby hindering glycerol attachment [10,39], while it decreases after the attainment of maximum solketal yield of 94.1% at 6 wt.% catalyst loading (Fig. 10b) due to a reduction in mass transfer [24]. The influence of time on the yield of solketal was examined by altering catalyst loading over the range of 4–8 wt.% where solketal yield was observed to increase up to 6 wt. % catalyst loading while starts declining upon further increment despite an increase in reaction time as shown in Fig. 10c due to the reaction reaching equilibrium [22,39].

A numerical optimization technique in Design Expert was used to determine the ideal settings for three input variables to achieve the maximum desirability score of 1. The objective was to maximize the production of solketal, while adhering to the predetermined limits of the variable ranges. RSM-CCD approach was used to identify the best conditions within a specified range, and according to it, the optimal solketal production was achieved using ultrasonic assistance, yielding a solketal output of 97. 2%. This optimal condition was then tested in the laboratory three times, resulting in an average solketal yield of 95.7%.

Characterization of solketal

The ideal parameters for the acetalization of glycerol were given by the RSM-CCD technique. Here, a reaction duration of 14 min, ace:gly molar ratio of 7.5:1, and catalyst loading of 5.7 wt.% predicted a yield of 96.8%, additionally, when the given parameters were tested in the laboratory, a 98.4% conversion of glycerol and 95.7% yield of solketal was attained through the acetalization reaction as confirmed by GC–MS analysis (Fig. 11) along with a 4.3% 1, 3-dioxane, 2, 2, dimethyl-5-hydroxy yield (six-membered) (Table 3) demonstrating that the value of the suggested regression model is reliable for promoting the acetalization process. Finally, the produced solketal was studied by NMR analysis. Spectroscopic measurements of the ^{1}H NMR spectrum (Fig. 12) confirmed that the product has both 2,2-dimethyl-1,3-dioxolane-4-methanol (major) and 6-membered ring 2,2-dimethyl-1,3-dioxan-5-ol (minor). In the ^{1}H NMR (500 MHz, $CDCl_3$) spectrum, two different singlets represent the six-methyl hydrogen of 1,3-dioxolane of the glycerol acetalization product at δ 1.33 and δ 1.26 ppm. The six-membered ring product was confirmed by the peaks at δ 1.34 and δ 1.23 representing another six-methyl hydrogens. Meanwhile, the broad singlet peak for the corresponding hydroxyl appears at δ 2.69 ppm. The –CH and $–CH_2$ groups present in both products are represented by peaks at δ 4.15–3.01 ppm [10].

Heterogeneity test and test for reusability

The as-prepared catalyst was tested for heterogeneity using the Hot Sheldon filtration method [10]. The reaction mixture was kept for ultrasonication for 10 min (under the optimal conditions outlined by RSM), which included an ace:gly molar ratio of 7.5:1, and a catalyst loading of 5.7 wt.%, a solketal yield of 87.53 ± 1.4% was achieved (Fig. 13a). Subsequently, the reaction was continued for an additional 6 min without the catalyst (after filtration). It was noted that the solketal yield increased by 3.12%. This result suggests the persistent presence of residual catalyst components in the reaction mixture, contributing to the improved conversion of glycerol to solketal yield and thereby confirming the catalyst's heterogeneity.

For economic efficiency, the recycling of catalysts must be studied as it enables resource reuse, leading to reduced manufacturing costs and complexity. The reusability of the current CND-SO_3H catalyst was evaluated under optimal reaction conditions. After completing every reaction cycle, the catalyst underwent a simple filtration process and was then rinsed alternately with chloroform and acetone, followed by overnight drying. Figure 13b illustrates the performance across cycles 1–7, showing a slight decline in glycerol conversion after the sixth cycle (82.1 ± 0.6%). In the seventh cycle, a further reduction in yield was observed (82.1 ± 0.6%), potentially due to pore clogging, surface poisoning by acetone and glycerol, and/or leaching of sulfonic acid content. A similar observation was also detected in our previous work [10,16].

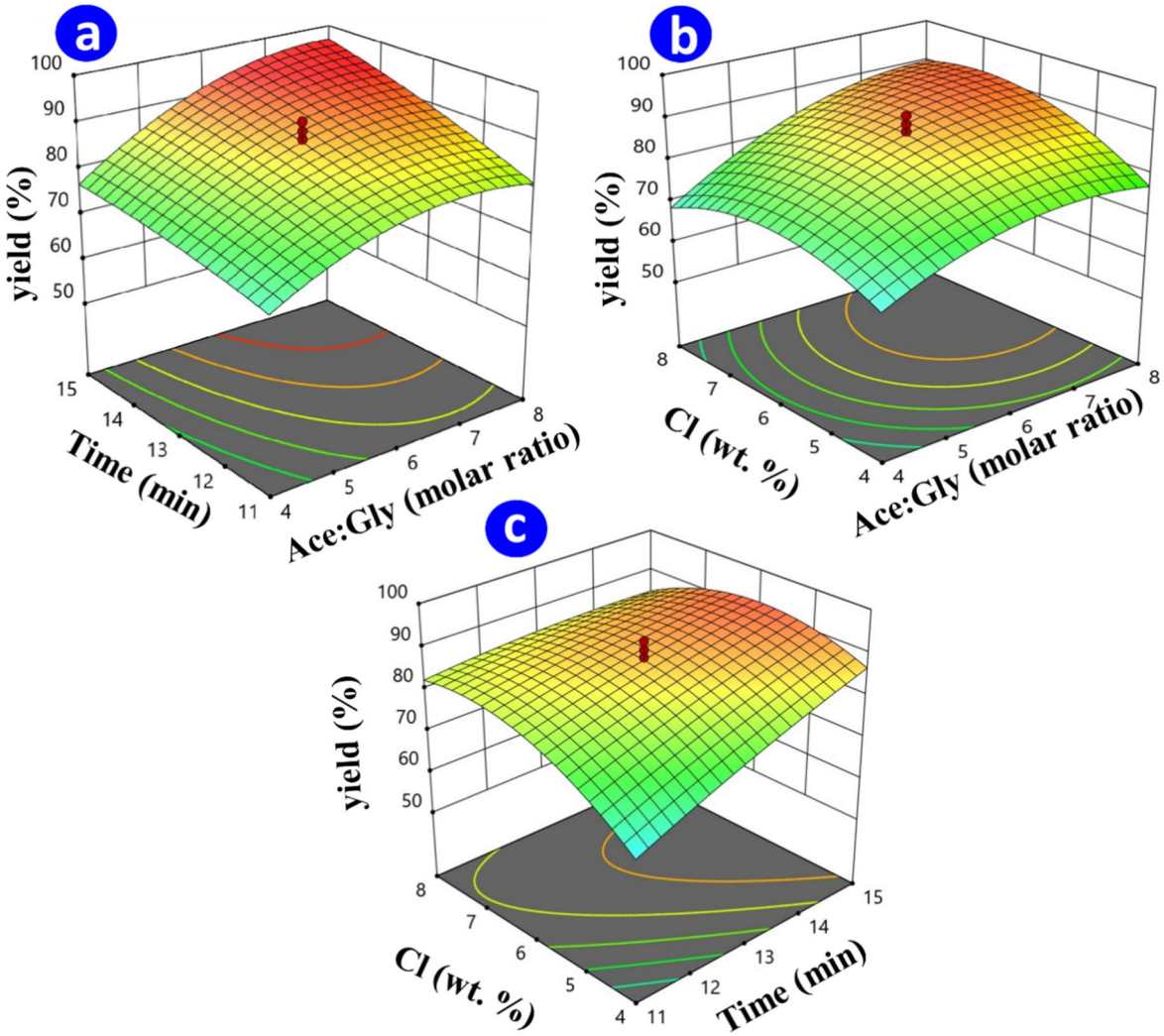

Figure 10. 3-D face diagram illustrating the relationship between the individual variables A–C illustrates the efficiency of the ultrasonication method for glycerol solketal synthesis.

Performance comparison of CND-SO_3H catalyst with previously reported catalysts for glycerol acetalization to produce solketal

The efficiency of our recently reported catalyst was studied in comparison to select heterogeneous catalysts used in the acetalization reaction for solketal production. Table 4 presents a comprehensive overview of relevant data, encompassing catalyst types, feedstocks, reaction conditions, turnover frequency (TOF), catalyst reusability cycles, and solketal yield. TOF, serving as a parameter to gauge intrinsic activity, offers insights into a catalyst's effectiveness for a given reaction[40]. Our reported catalyst demonstrated a TOF of 0.078 mol/g h, surpassing the performance of several specified catalysts listed in Table 4, thereby establishing its superior activity in the acetalization process. Catalysts like HR/Y-F127 [41], UAV-59 [42], G-ASA [43], NbP [44], GS-SO_3H [45], MOR 0.5 [46], AC-PMfs [47], Silica-coated Fe_3O_4 magnetic NPs [19], Mil-118-SnO_2 [48] though have high catalyst activity (high conversion) require a long reaction time and temperature to produce solketal. Also, despite having a higher TOF than the current catalyst, SAFACAM [10] and Sulfated ZrO_2 [24] catalyst, exhibited significant disadvantages, such as extended reaction times and a low solketal yield. Beyond most of the catalysts documented in Table 4, the current catalyst in particular has a high solketal yield in a short reaction time with seven cycles of reusability.

Life cycle cost analysis of solketal production using CND-SO_3H catalyst

The economic and productive viability of commercializing the acetalization process for large-scale solketal production is significantly influenced by the catalyst's cost-effectiveness and effective performance. The expenses

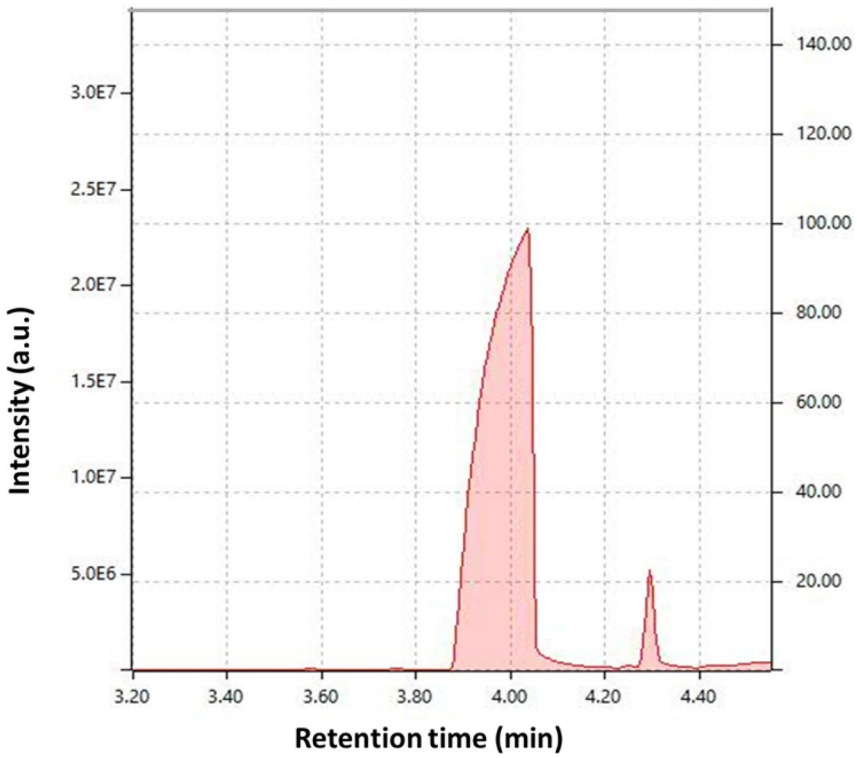

Figure 11. GC–MS plot graph of our synthesized product.

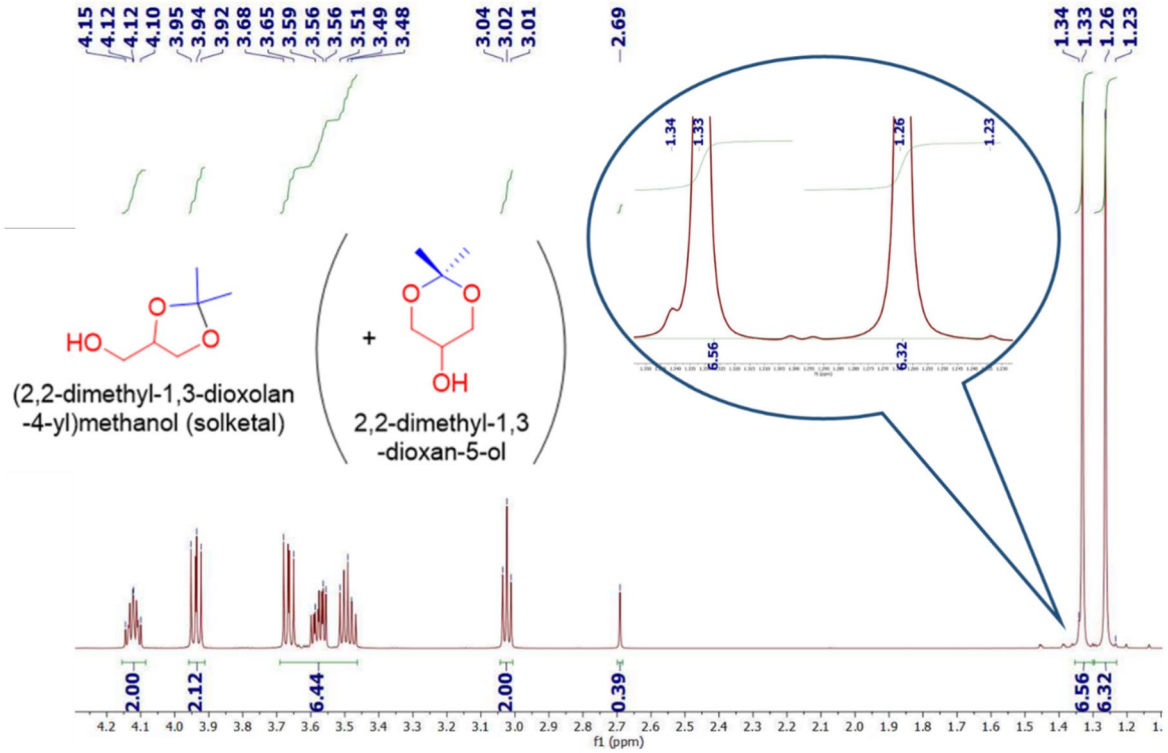

Figure 12. ^{1}H NMR spectra at 28 °C in $CDCl_3$ of the product of glycerol acetalization using the CND-SO_3H catalyst.

Peak	Retention time	Area (%)	Name
1	4.033	95.7	Solketal
2	4.294	4.3	2, 2, dimethyl-1, 3-dioxane, -5-ol

Table 3. GC–MS result of the acetalization reaction.

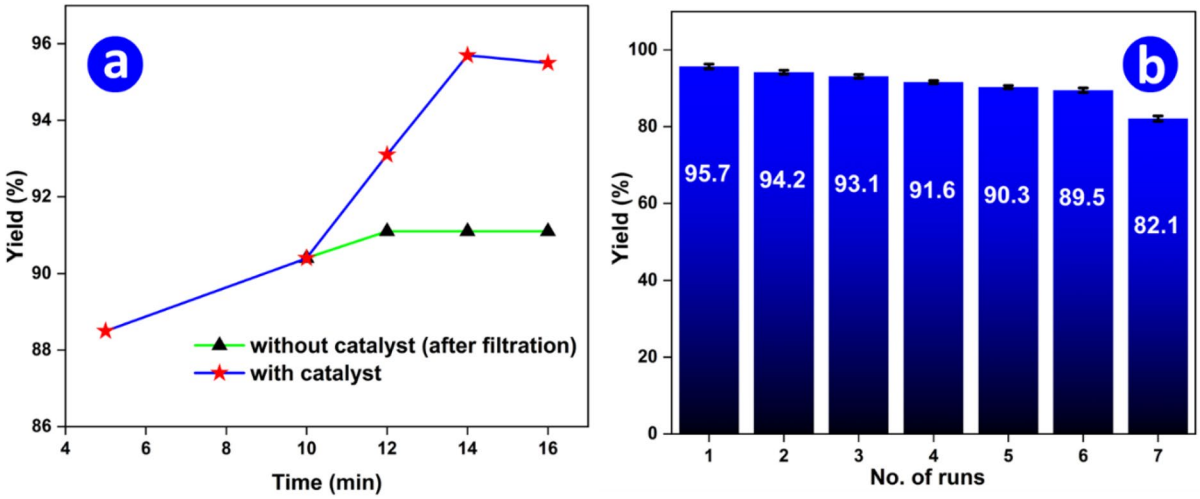

Figure 13. (**a**) Heterogeneity test of CND-SO_3H up to 16 min reaction duration and (**b**) Reusability graph of CND-SO_3H in the acetalization (yield) of glycerol over 7 cycles.

Entry	Catalyst	Reaction method	Conditions[a]	Conversion/Yield (%)	Selectivity (%)	Reusability (% C)	TOF (mol/g h)[b]	Refs.
1.	HR/Y-F127	Conventional	20:1, 2 h, 10, 55	100 (Y)	98	5 (95)		41
2.	UAV-59	Conventional	10:1, 2 h, 5, 55	90 (C)	98	5 (84)		42
3.	G-ASA	Conventional	4:1, 1 h, 0.5, RT	95.8 (C)	96.8	3 (96)		43
4.	NbP	Conventional	5:1, 4 h, 0.3 g, 120	94 (C)	100	–	–	44
5.	SAFACAM	Microwave	5:1, 10, 8, 70	98.1(C)	100	6 (82.3 ± 0.2)	0.79	10
6.	GS-SO_3H	Conventional	4:1, 240, 5, RT	91 (C)	98	4 (–)	0.05	45
7.	MOR 0.5	Conventional	10:1, 4 h, 0.5 g, 60	100 (Y)	99	3 (> 90)		46
8.	Silica-coated Fe_3O_4 magnetic NPs	Ultrasonication	5:1, 15, 5, 28	97 (C)	100	5 (95)	0.84	19
9.	Zirconium organophosphate	Conventional	10:1, 180, 5, 40	90.2 (C)	98.5	5 (87.5)	0.63	40
10.	Sulfated ZrO_2	Conventional	6:1, 60, 0.6, 40	80 (C)	88	4 (–)	1.47	24
11.	AC-PMfs	Conventional	4:1, 5 h, 1.6, 55	81 (C)	98	4 (75)		47
12.	Mil-118-SnO_2	Conventional	10:1, 4 h, 0.04, Reflux	76 (C)	97	5(97)		48
13.	CND-SO_3H	Ultrasonication	7.5:1, 14, 5.7, RT	95.7 (Y)	95.7	7 (82.1)	0.78	This work

Table 4. Comparison of the current CND SO_3H catalyst with previously reported solketal synthesis catalysts. [a]acetone:glycerol molar ratio, reaction time (min), catalyst loading (wt. %), temperature (°C). [b]TOF, moles of glycerol converted per gram of catalyst per hour; RT, room temperature; HR/Y-F127, Hierarchical Faujasite zeolite; UAV-59, $[Gd(H_4nmp)(H_2O)_2]Cl_2H_2O$; G-ASA, aminosulfonic acid-derivatized graphene; SAFACAM, sulfonic acid functionalized aromatic carbon access material; GS-SO_3H, glucose surfactant-SO_3H; MOR 0.5, mordenite 0.5; AC-PMFs, activated carbon -petiole of Mauritia flexuosa.

related to the synthesis of catalyst and solketal manufacturing must be taken into account to assess the possible applicability and viability of both the catalyst and the synthesized product, as well as to address the steadily increasing need for energy. The reusability of the catalyst can impact the overall production cost significantly. Thus, careful selection of readily available waste precursor materials from nature is crucial for both catalyst and solketal production, given their undeniable advantages. The cost estimation performed for catalyst preparation in this study serves as a critical tool for assessing method feasibility. It considers various factors including raw material sourcing, production methods, necessary treatment processes, and notably, the reusability factor,

which greatly influences overall expenses. The findings, detailed in Tables 5 and 6, present the cost observations per kilogram of sulfonated catalyst, expressed in US dollars ($). Cost of raw materials are as per the purchased quotation price (2023–2024) from India Mart and Sisco Research Lab, India. 1 USD = 83.34 INR (May 2024).

The authors conducted this LCCA using glycerol, a commercially available starting material, to provide readers with a general understanding of the overall synthesis of solketal for commercial applicability. Ultimately, the cost of crude glycerol from companies can be disregarded and glycerol can be synthesized directly from factories through direct purification and distillation from the biodiesel industry, which will significantly lower the market prices and contribute to the sustainability of the biofuel sector.

Conclusion

This study presents the synthesis of a novel heterogeneous functionalized carbon nanodot catalyst from lotus leaf extract, exhibiting high efficiency in solketal production with a remarkable turnover frequency (TOF) of 0.78 mol/g h. Switching from conventional heating to ultrasonication shortened the reaction time to only 14 min

Approximate cost estimation for 100 kg catalyst production		
Step	**Description**	**Amount**
Cost of starting material (CSM)	Biomass waste is gathered from NIT Silchar campus. 15% cost factored in for industrial-scale operations	$0
Cost of size reduction (CSR)	Manual reduction was done for batch studies. 15% extra costs are assigned for machine reduction	$0
Cost of drying raw material (CDR) + Cost of reflux (CF) +	Time in hour × consumed unit × cost/unit = 10 × 1 × $0.041	$0.41
Total estimated cost of raw material (CRM):	CSM + CSR + CDR + CF = $0 + $0 + $0.41	$0.41
Impregnation cost (IC) = Chemicals used (CU) + Chemicals cost (CC) + Electricity consumed (EC)	CC = [H_2SO_4 quantity needed (L) × cost/L] = 1000 × $1.45 = $1450 EC = Time (hour) × consumed unit × cost/unit = (24 × 1 × $0.041) = $0.984 IC = $1450 + $0.0984	1450.098
Washing cost (WC)	WC = units consumed × unit cost for 1 L water = 1 × $0.041	$0.041
Drying cost (DC)	DC = Time in hour × consumed unit × cost/unit = 10 × 1 × $0.041	$0.41
Net cost	CRM + IC + WC + DC = $0.41 + $1450.098 + $0.041 + $0.41	$1450.959
Cost of catalyst (100 kg)	= Net cost + overhead costs (15% of extra cost) = $1450.959 + $217.64	$1668.6
Cost of (1 kg) catalyst	= Cost of catalyst (100 kg)/100	$16.686
Cost of (1 kg) catalyst after recycling	Cost of one-time use /no. of use in reusability = $16.686/7	$2.38

Table 5. Costs of preparing catalysts step-by-step.

Step	Description	Cost
Cost of crude glycerol to produce 100 kg solketal	Amount (kg) × glycerol cost per kg = 105 kg × $0.19 = 19.95	$19.95
Cost of catalyst to produce 100 kg of solketal	Amount (kg) × catalyst cost per kg = 5.98 × $2.38	$14.23
Cost of acetone required to produce 100 kg of solketal	After 7 recycle, the acetone cost for production of 100 kg of solketal = (amount (kg) × acetone cost per kg) ÷ 7 = (496 × $0.38) ÷ 7 = $26.92	$26.92
Production cost of solketal ((acetalization time (h) × units × per unit cost)	= 0.24 h × 1 × $0.041 = 0.014	$0.014
Extra charges (cost of washing + multifarious)	$1.40	$1.40
Cost of solketal (100 kg)	$19.95 + $14.23 + $26.92 + $0.014 + $1.40	$62.514
Overhead cost[a] (15% of net cost)	$9.377	$9.377
Solketal cost (100 kg)	$62.514 + $9.377	$71.891
Solketal cost (1 kg)	$0.719	$0.719

Table 6. Estimated cost associated with solketal production (100 kg). [a]Overhead cost in solketal production = 15% of the net charge and includes indirect expenses such as administrative, utility, and facility costs. Disclaimer: The present cost analysis might not accurately reflect the actual expenses that could arise at a commercial scale. However, it provides an estimated cost and serves as a valuable reference for future researchers.

while attaining an excellent solketal yield of 95.7%. Notably, the catalyst demonstrates durability over multiple acetalization cycles, maintaining 82.1% product yield after seven reaction cycles. Utilizing RSM, we optimized the operational parameters, identifying ace:gly molar ratio as the most influential factor for enhancing the acetalization performance. Furthermore, our study on LCCA indicated a significant cost advantage for biomass-derived catalysts over market alternatives, making solketal production economically viable for industrial-scale implementation and trade, particularly considering the favorable cost comparison with solketal $0.719 per kg. These results provide a promising pathway for the commercialization and widespread adoption of this sustainable catalyst technology.

Data availability

Data will be made available on a reasonable request to the corresponding author.

Received: 22 March 2024; Accepted: 6 August 2024
Published online: 29 August 2024

References

1. Ashraf, H. & Karahan, B. D. Biowaste valorization into valuable nanomaterials: Synthesis of green carbon nanodots and anode material for lithium-ion batteries from watermelon seeds. *Mater. Res. Bull.* **169**, 112492 (2024).
2. Xu, X. *et al.* Electrophoretic analysis and purification of fluorescent single-walled carbon nanotube fragments. *J. Am. Chem. Soc.* **126**, 12736–12737 (2004).
3. Hassanvand, Z., Jalali, F., Nazari, M., Parnianchi, F. & Santoro, C. Carbon nanodots in electrochemical sensors and biosensors: A review. *ChemElectroChem* **8**, 15–35 (2021).
4. Latif, Z. *et al.* Carbon quantum dots (CQDs)-modified polymers: A review of non-optical applications. *Nanoscale* **16**, 2265–2288 (2024).
5. Nguyen, T. N., Le, P. A. & Phung, V. B. T. Facile green synthesis of carbon quantum dots and biomass-derived activated carbon from banana peels: Synthesis and investigation. *Biomass Convers. Biorefinery* **12**, 2407–2416 (2022).
6. Ruatpuia, J. V. *et al.* Green biodiesel production from Jatropha curcas oil using a carbon-based solid acid catalyst: A process optimization study. *Renew. Energy* **206**, 597–608 (2023).
7. Gouda, S. P., Dhakshinamoorthy, A. & Rokhum, S. L. Metal-organic framework as a heterogeneous catalyst for biodiesel production: A review. *Chem. Eng. J. Adv.* **12**, 100415 (2022).
8. Yin, P. *et al.* Effects of Scenedesmus dimorphus, spirulina biodiesel, hydrogen and nanoparticles fuel blends on mass burn fraction, emission, noise and vibration characteristics. *Fuel* **352**, 129010 (2023).
9. Kushwaha, T. *et al.* Esterification of oleic acid to biodiesel using biowaste-based solid acid catalyst under microwave irradiation. *Environ. Prog. Sustain. Energy* **2023**, 14170 (2023).
10. Ao, S. *et al.* Microwave-assisted valorization of glycerol to solketal using biomass-derived heterogeneous catalyst. *Fuel* **345**, 128190 (2023).
11. Ao, S. & Rokhum, S. L. Recent advances in the valorization of biodiesel by-product glycerol to solketal. *J. Chem.* **2022**, 1–18 (2022).
12. Das, A., Shi, D., Halder, G. & Lalthazuala Rokhum, S. Microwave-assisted synthesis of glycerol carbonate by transesterification of glycerol using Mangifera indica peel calcined ash as catalyst. *Fuel* **330**, 125511 (2022).
13. Gomes, P. *et al.* Green production of biodiesel from high acid value oil via glycerol esterification and transesterification catalyzed by nano hydrated eggshell-derived CaO. *Energies* **16**, 6717 (2023).
14. Guerra, F. B., Cavalcante, R. M. & Young, A. F. Green propylene and polypropylene production from glycerol: Process simulation and economic evaluation. *ACS Sustain. Chem. Eng.* **11**, 2752–2763 (2023).
15. Subhash, M., Pal, D. B. & Jana, S. K. Biofuels additives derived via clay supported heteropoly acid catalyzed etherification of glycerol with t-butanol-biomass to liquid oxygenates. *Chem. Pap.* **76**, 775–784 (2022).
16. Saikia, K. *et al.* Sulphonated biomass-based catalyst for solketal synthesis by acetalization of glycerol—a byproduct of biodiesel production. *Fuel Process. Technol.* **238**, 107482 (2022).
17. Wang, H., Cui, Y., Shi, J., Tao, X. & Zhu, G. Porous carbon supported Lewis acid-base sites as metal-free catalysts for the carbonylation of glycerol with urea. *Appl. Catal. B Environ.* **330**, 122457 (2023).
18. Meng, F. *et al.* Carbon-based metal-free catalysts for selective oxidation of glycerol to glycolic acid. *Chem. Eng. Sci.* **268**, 118394 (2023).
19. Rajkumari, K. *et al.* A reusable magnetic nanocatalyst for bio-fuel additives: The ultrasound-assisted synthesis of solketal. *Sustain. Energy Fuels* **5**, 2362–2372 (2021).
20. Laskar, I. B., Rajkumari, K., Gupta, R. & Rokhum, L. Acid-functionalized mesoporous polymer-catalyzed acetalization of glycerol to solketal, a potential fuel additive under solvent-free conditions. *Energy Fuels* **32**, 12567–12576 (2018).
21. Huang, Y., Zhang, G. & Omega, Q.Z.-A. Preparation of the WOX/MCM-41 solid acid catalyst and the catalytic performance for solketal synthesis. *ACS Publ.* **6**, 3883 (2021).
22. Moreira, M. N., Faria, R. P. V., Ribeiro, A. M. & Rodrigues, A. E. Solketal production from glycerol ketalization with acetone: Catalyst selection and thermodynamic and kinetic reaction study. *Ind. Eng. Chem. Res.* **58**, 17746–17759 (2019).
23. Noor Armylisas, A. H., Hoong, S. S., Tuan Noor Maznee, T. I., Yeong, S. K. & Mohammat, M. F. Solventless transacetalization of solketal over Amberlyst catalysts into valuable bio-based chemicals. In *Wiley Online Libr. Noor Armylisas, SS Hoong, TI Tuan Noor Maz. SK Yeong, MF MohammatJournal Chem. Technol. Biotechnol., vol. 96* 2667–2674 (Wiley, 2021).
24. Vannucci, J. A., Nichio, N. N. & Pompeo, F. Solketal synthesis from ketalization of glycerol with acetone: A kinetic study over a sulfated zirconia catalyst. *Catal. Today* **372**, 238–245 (2021).
25. Rokhum, S. L., Changmai, B., Kress, T. & Wheatley, A. E. H. A one-pot route to 1 tunable sugar-derived sulfonated carbon catalysts 2 for sustainable production of biodiesel by fatty acid esterification. *Renew. Energy* **1481**, 01720–01721 (2021).
26. Devasan, R. *et al.* Microwave-assisted biodiesel production using bio-waste catalyst and process optimization using response surface methodology and kinetic study. *Sci. Rep.* **13**, 1–17 (2023).
27. Ao, S. *et al.* Active sites engineered biomass-carbon as a catalyst for biodiesel production: Process optimization using RSM and life cycle assessment. *Energy Convers. Manag.* **300**, 117956 (2024).
28. Jamil, F. *et al.* Valorization of waste "date seeds" bio-glycerol for synthesizing oxidative green fuel additive. *J. Clean. Prod.* **165**, 1090–1096 (2017).
29. Kefas, H. M., Yunus, R., Rashid, U. & Taufiq-Yap, Y. H. Modified sulfonation method for converting carbonized glucose into solid acid catalyst for the esterification of palm fatty acid distillate. *Fuel* **229**, 68–78 (2018).
30. Ngafwan, N. *et al.* Study on novel fluorescent carbon nanomaterials in food analysis. *Food Sci. Technol.* **42**, 1456 (2022).
31. Thommes, M. *et al.* Physisorption of gases, with special reference to the evaluation of surface area and pore size distribution (IUPAC Technical Report). *Pure Appl. Chem.* **87**, 1051–1069 (2015).

32. Onat, E., Sait Izgi, M., Şahin, Ö. & Saka, C. Highly active hydrogen production from hydrolysis of potassium borohydride by caffeine carbon quantum dot-supported cobalt catalyst in ethanol solvent by hydrothermal treatment. *Int. J. Hydrogen Energy* **1**, 456 (2023).
33. Ao, S. *et al.* Synthesis and utilization of biomass-derived sulfonated heterogeneous catalyst-BT-SO3H for microalgal biodiesel production. *Environ. Res.* **245**, 118025 (2024).
34. Betiku, E., Anietie, H., Etim, O., Pereao, O. & Ojumu, T. V. Two-step conversion of neem (*Azadirachta indica*) seed oil into fatty methyl esters using a heterogeneous biomass-based catalyst: An example of cocoa pod husk. *Energy Fuels* **31**, 46 (2017).
35. Selvaraj, R., Moorthy, I. G., Kumar, R. V. & Sivasubramanian, V. Microwave mediated production of FAME from waste cooking oil: Modelling and optimization of process parameters by RSM and ANN approach. *Fuel* **237**, 40–49 (2019).
36. Marzouk, M. N. *et al.* Process optimization of biodiesel production via esterification of oleic acid using sulfonated hierarchical mesoporous ZSM-5 as an efficient heterogeneous catalyst. *J. Environ. Chem. Eng.* **9**, 105035 (2021).
37. Sharma, A., Kodgire, P. & Kachhwaha, S. S. Biodiesel production from waste cotton-seed cooking oil using microwave-assisted transesterification: Optimization and kinetic modeling. *Renew. Sustain. Energy Rev.* **116**, 109394 (2019).
38. Kodgire, P., Sharma, A. & Kachhwaha, S. S. Optimization and kinetics of biodiesel production of *Ricinus communis* oil and used cottonseed cooking oil employing synchronised 'ultrasound + microwave' and heterogeneous CaO catalyst. *Renew. Energy* **212**, 320–332 (2023).
39. Kowalska-Kuś, J., Held, A. & Nowińska, K. A continuous-flow process for the acetalization of crude glycerol with acetone on zeolite catalysts. *Chem. Eng. J.* **401**, 126143 (2020).
40. Li, X., Jiang, Y., Zhou, R. & Hou, Z. Acetalization of glycerol with acetone over appropriately-hydrophobic zirconium organophosphonates. *Appl. Clay Sci.* **189**, 105555 (2020).
41. Sadjadi, S., Tarighi, S., Delangiz, M. & Heravi, M. Heteropolyacid supported on ionic liquid decorated hierarchical faujasite zeolite as an efficient catalyst for glycerol acetalization to solketal. *Sci. Rep.* **13**, 1–12 (2023).
42. Santos-Vieira, I. C. M. S., Mendes, R. F., Almeida Paz, F. A., Rocha, J. & Simões, M. M. Q. Acetalization of glycerol with acetone over UAV-59 catalyst: Mild reaction conditions and enhanced selectivity. *Catal. Today* **424**, 114296 (2023).
43. Poulose, C. A. *et al.* Acidic graphene organocatalyst for the superior transformation of wastes into high-added-value chemicals. *Nat. Commun.* **14**, 1–10 (2023).
44. Ginjupalli, S. R., Balla, P. K., Ramachandra-Prabhu, C., Pethan-Rajan, N. & Pothu, R. Acid catalysed glycerol transformation to fuel additives over different metal phosphate solid acid catalysts. *Biomass Convers. Biorefinery* **13**, 12749–12761 (2023).
45. Ghosh, A. *et al.* A green approach for the preparation of a surfactant embedded sulfonated carbon catalyst towards glycerol acetalization reactions. *Catal. Sci. Technol.* **10**, 4827–4844 (2020).
46. Saini, B., Tathod, A. P., Saxena, S. K., Arumugam, S. & Viswanadham, N. Sustainable upgrade of bioderived glycerol to solketal through acetalization over metal-free mordenite catalysts. *ACS Sustain. Chem. Eng.* **10**, 1172–1181 (2022).
47. Balotin, G. *et al.* Upgrading catalytic efficiency of activated carbons by tailoring lignocellulosic biomass waste for sustainable conversion of glycerol to solketal. *Mol. Catal.* **538**, 112976 (2023).
48. Dashtipour, B., Dehghanpour, S. & Sharbatdaran, M. Improvement of the acidic properties of MOF by doped SnO2 quantum dots for the production of solketal. *J. Chem. Sci.* **134**, 4 (2022).

Acknowledgements

The authors gratefully acknowledge SAIFs (IITP, IIT Delhi, IIT Bombay) and CIF NIT SILCHAR for analyses.

Author contributions

Supongsenla Ao: Conceptualization, methodology, investigation, data curation, manuscript writing, Shiva Prasad Gouda: Data curation, writing reviewing & editing, Lakshi Saikia: Data curation, writing reviewing & editing. Baskar Gurunathan: Writing reviewing & editing, Samuel Lalthazuala Rokhum: Investigation, supervision, writing reviewing & editing.

Competing interests

The authors declare no competing interests.

Additional information

Supplementary Information The online version contains supplementary material available at https://doi.org/10.1038/s41598-024-69553-7.

Correspondence and requests for materials should be addressed to S.L.R.

Reprints and permissions information is available at www.nature.com/reprints.

Publisher's note Springer Nature remains neutral with regard to jurisdictional claims in published maps and institutional affiliations.